Phase Distribution Efficiency of cm-Scale Ultrasonically Powered Receivers

Saccher, Marta; Rashidi, Amin; Savoia, Alessandro Stuart; Giagka, Vasiliki; Dekker, Ronald

Citation (APA)
Saccher, M., Rashidi, A., Savoia, A. S., Giagka, V., & Dekker, R. (2023). Phase Distribution Efficiency of cm-Scale Ultrasonically Powered Receivers. In *Proceedings of the 2023 IEEE International Ultrasonics Symposium (IUS)* IEEE. https://doi.org/10.1109/IUS51837.2023.10307986

Important note
To cite this publication, please use the final published version (if applicable).
Please check the document version above.

Phase Distribution Efficiency of cm-Scale Ultrasonically Powered Receivers

Marta Saccher*, Amin Rashidi*, Alessandro Stuart Savoia†, Vasiliki Giagka*‡ and Ronald Dekker*§

*Department of Microelectronics, Delft University of Technology, Delft, The Netherlands
†Department of Industrial, Electronic, and Mechanical Engineering, Roma Tre University, Rome, Italy
‡Department of System Integration and Interconnection Technologies, Fraunhofer IZM, Berlin, Germany
§MEMS & Micro Devices, Philips, Eindhoven, The Netherlands

Abstract—In the domain of ultrasonically powered biomedical implants, there is an increasing interest in cm-scale ultrasonic receivers (RX). However, when a single-element transducer is used as the RX transducer, an uneven phase distribution across the RX area can significantly reduce the harvestable power. In this paper, we investigate the impact of lateral and angular misalignment on the acoustic field phase distribution across the RX surface. We show that, for a single-element RX transducer, lateral misalignment has minimal effect on the harvestable power, whereas even small angular misalignments can cause a considerable reduction, especially for larger RX sizes. We present a potential solution that consists of subdividing a large RX transducer (e.g. $20 \times 20\,\mathrm{mm}^2$) into smaller elements, which significantly improves power transfer efficiency by taking advantage of the smaller phase variation across the surface of each element. The trade-offs between achieving a minimum acceptable power transfer efficiency and managing the increased complexity in packaging and matching circuitry are also discussed.

Index Terms—phase distribution efficiency, ultrasonic receivers, ultrasound power transfer, receiver partitioning

I. Introduction

Implantable bioelectronics have revolutionised patient lives by delivering localised and on-demand therapies. Pacemakers, cochlear implants, and deep brain stimulators are some of the successfully commercialised examples. More recently, there is a growing interest in battery-less implementations of biomedical implants due to higher safety, the possibility of miniaturisation, and patient comfort [1]. Depending on the application, these implants have different power requirements ranging from a few microwatts for sensing applications [2], to tens of milliwatts for high-density stimulation backends [3].

Among the different powering methods for wireless implants, ultrasonic power links have demonstrated superior scalability when using micromachined transducers [2], [4]–[6], and low energy losses in soft tissue (around $0.6\,\mathrm{dB/(cm\,MHz)}$). In addition, the ultrasound beam can be precisely focused on the target receiver by using phased arrays, minimising the power losses in the areas surrounding the receiver [7].

Although most of the reported ultrasonically power implants have a micro- or millimetre-scale receiving aperture [2], [4], [5], [8], in some cases, the high power demands

of the application require cm-scale receivers. For instance, [9] demonstrates the first monolithic integration of power-receiving PMUT on an ASIC, at the cost of a low aperture efficiency. To compensate for the low efficiency, they use an aperture area $30\,\mathrm{mm}^2$ large. In [10], an array of 36 parallel single-element piezoelectric crystals with a total aperture area of $1.3\,\mathrm{cm}^2$ is used to deliver $280\,\mathrm{mW}$ to power a deep brain stimulator. However, in the previously reported research, a single-element transducer was used as the receiver (RX). When the phase distribution across the RX area is uneven, the harvestable power significantly decreases.

In this paper, we investigate the impact of lateral and angular misalignment on the phase distribution of the acoustic field across the RX surface. We evaluate its effect on the harvestable power as a function of RX areas ranging from mm^2 to cm^2. We assess the use of transducer arrays as RX, as a solution to improve the power transfer efficiency.

II. Basic Concept

In Fig. 1(a) the phase of the ultrasound field produced by a single element TX transducer with a $39\,\mathrm{mm}$ diameter and $2.5\,\mathrm{MHz}$ centre frequency is shown at different planes parallel to the surface of the TX. The planes are located at $10\,\mathrm{mm}$, $50\,\mathrm{mm}$, and $100\,\mathrm{mm}$, to represent the location of a RX transducer in the body. The figure shows that, for diameters smaller than the one of the TX transducer, the phase distribution is rather uniform. However, in a realistic scenario, where the TX is placed outside of the body, and the RX is in the body, perfect alignment between the two will rarely occur, and lateral and angular misalignment will be present. This scenario is depicted in Fig. 1(b), where the plane is tilted by $15°$ with respect to the TX surface. It can be observed that the phase distribution of the ultrasound field is uneven across the entire surface. In this condition, each point on the RX surface is at a different distance from the TX surface. Therefore, the ultrasound wave hits the different points on the surface of the RX at a different time, causing a phase difference compared to the parallel configuration. In Fig. 1(c), the pressure waves at different points on the RX surface are shown for the perfectly aligned case (top plot), and for a tilt of $5°$ (bottom plot). When using a single-element RX transducer, the usable harvested power originates from the coherent average of the pressure integrated across the RX
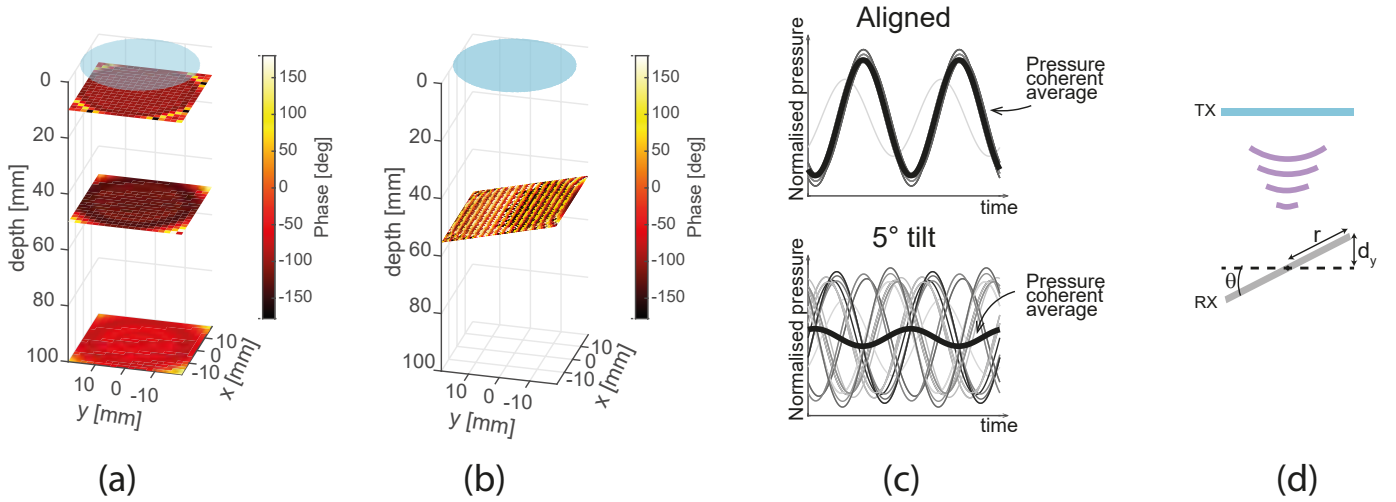
Fig. 1. (a) Simulation of phase distribution on planes parallel to the TX, located at 10 mm, 50 mm, and 100 mm. Blue circle indicates the TX transducer. (b) Simulation of phase distribution on a plane tilted by 15°, and located at 50 mm from TX. (c) Simulations of pressure waves at locations on a square RX transducer at 50 mm from the TX. (top) perfectly aligned case, (bottom) tilt of 5° with respect to the TX surface. Thick black line indicates the coherently averaged pressure across the RX surface. Driving conditions are the same for the aligned and tilted case. Data in (a to c) is obtained from ultrasound field simulations using FOCUS [11]. (d) Schematic representation of the effect of an angular misalignment between TX and RX.

surface (shown as a thicker trace in Fig. 1(c)). Comparing the top and bottom plots of Fig. 1(c), it can be observed that, due to the angular tilt, the pressure waves are shifted in time, causing a significantly lower pressure average, therefore lower usable power. Assuming that the acoustic wave impinging on the RX surface is planar, the difference in phase compared to the parallel case can be calculated with the following equation, which refers to Fig. 1(d):

$$d_y = r \cdot \sin(\theta)$$
$$\Delta_{phase} = \frac{\mathbf{d_y}}{c} \cdot f \cdot 360° \tag{1}$$

Where r is the distance from the centre of the RX transducer, θ is the tilt angle, c is the speed of sound in the medium, and f is the frequency. In addition, (1) shows that the larger the receiver, the greater the phase difference across its surface, which significantly reduces the benefit of using cm-scale receivers to harvest a higher amount of power.

A. Simulation of the ultrasound field

To understand the impact of lateral and angular misalignment on the phase distribution of the acoustic field across the RX surface, we simulated the ultrasound field generated by the TX transducer using FOCUS [11]. The TX transducer is a circular, single-element piston transducer with a 2.5 MHz centre frequency and 39 mm diameter. We simulated squared receivers, with sizes ranging from 4×4 mm^2 to 20×20 mm^2 and computed the harvestable power for various misalignment scenarios at different depths. We used water as the medium for the simulations.

III. RESULTS AND DISCUSSION

A. Lateral misalignment

Figure 2 shows the effect of lateral misalignment between TX and RX on the amount of harvestable power at the RX,

assuming that TX and RX are on parallel planes. In each of the plots of Fig. 2, the power at the RX is normalised with respect to the maximum harvestable power in the simulated area. As the area of the RX transducer increases, smaller lateral misalignments are tolerated to maintain similar efficiencies. For receiver size from 4×4 mm^2 to 20×20 mm^2, lateral misalignment up to 10 mm results in a power loss of less than 30 %. In addition, the position of the RX is usually approximately known, and larger lateral misalignment, especially of more than 20 mm, can be considered unlikely in a real case scenario. The results shown in Fig. 2, are for a distance between TX and RX of 50 mm. The results are comparable for 10 and 100 mm distance. Therefore, in these conditions, lateral misalignment does not significantly degrade the harvestable power. However, these observations depend on the diameter, geometry, and centre frequency of the TX transducer. At lower frequencies, the effect of the lateral misalignment is further reduced due to a larger wavelength because the phase difference between two points separated by a certain distance decreases as the wave period becomes longer.

B. Angular misalignment

Figure 3 shows the effect of angular misalignment on the harvestable power at the RX. The power at the RX is normalised with respect to the maximum power among the simulated conditions, which is for the perfectly aligned case. The power loss is very significant for RX with larger areas, where an angular misalignment of 1° already causes a drop of 25 % in the harvestable power with respect to the perfectly aligned case for a 20×20 mm^2 receiver (Fig. 3(a)). This is because the larger the area, the greater the phase difference across the RX, therefore the higher the power loss (see (1)). In addition, the effect of the angular tilt is comparable at different distances between TX and RX. However, by using a
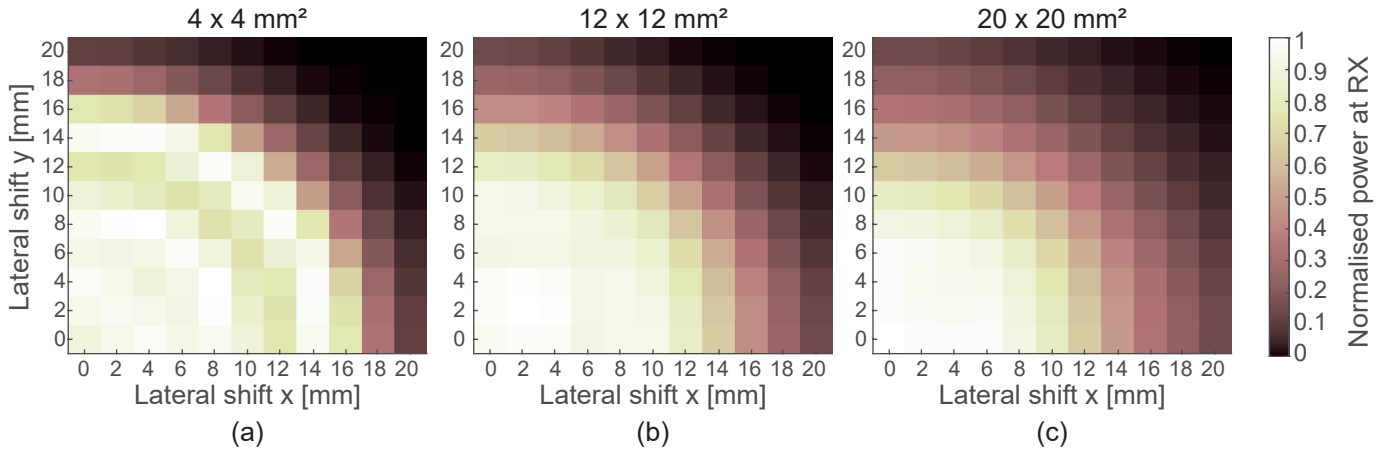
Fig. 2. Simulated normalised power at the RX with respect to a lateral shift between TX and RX at a distance of $50\,\mathrm{mm}$ between TX and RX transducer. (a) $4 \times 4\mathrm{mm}^2$ RX. (b) $12 \times 12\mathrm{mm}^2$ RX. (c) $20 \times 20\mathrm{mm}^2$ RX.

TX with a lower frequency, the effect of the angular tilt can be mitigated due to the larger wavelength, therefore smaller phase difference between points on the RX surface (Fig. 3(b)).

C. Example of power at RX

Subsequently, we measured the pressure profile of a single-element PZT piston transducer with a $2.25\,\mathrm{MHz}$ centre frequency and $39\,\mathrm{mm}$ diameter, by driving it at $2.5\,\mathrm{MHz}$. We used a needle hydrophone mounted on a motorised stage and scanned a plane at 50 and $100\,\mathrm{mm}$ distance, while the transducer was tilted by $1.3°$ with respect to the scanning plane. Figure 4 shows the available and usable power at the receiver, where "available power" is the power computed by integrating the acoustic intensity over the RX surface, and "usable power" is the power associated with the acoustic pressure coherently averaged over the RX surface. The power was calculated for squared ultrasound receivers with lateral size ranging from $2\,\mathrm{mm}$ to $20\,\mathrm{mm}$, assuming they would be positioned in the plane scanned by the needle hydrophone. Since the phase
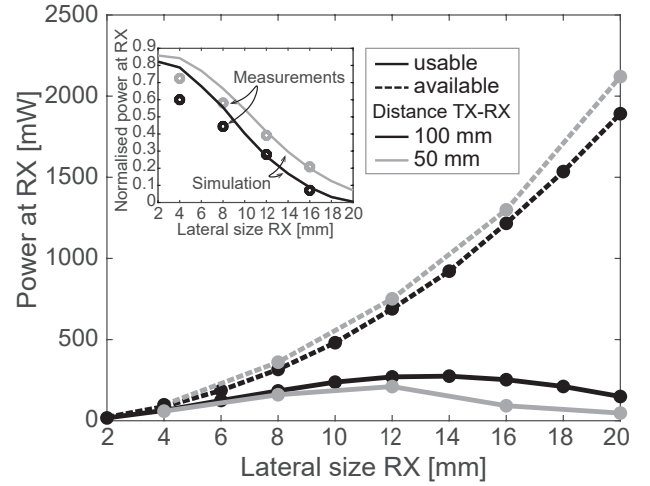

Fig. 4. Calculated usable and available power at RX depending on the lateral size of the RX, at a distance of 50 and $100\,\mathrm{mm}$, when TX is tilted by $1.3°$ with respect to the scanning plane. (inset) Power loss with respect to the available power at the RX due to angular misalignment, and comparison with simulation.

distribution in planes parallel to the TX is rather uniform for diameters smaller than the one of the TX, as shown in Fig 1(a), the available power increases with increasing receiver size. However, because of the angular misalignment between TX and RX, the usable power significantly decreases for bigger RX sizes. In addition, the inset in Fig. 4 shows the power loss due to the TX angular misalignment of $1.3°$, with respect to the available power, for different RX sizes. The plot inset presents measurements and simulations in good agreement, with a slight deviation for smaller receiver sizes.

D. Partitioning the receiver

A possible solution to mitigate the effect of the power loss due to misalignment is to partition the RX transducer [12]. In practice, this consists in using a transducer array instead of a single-element. By doing this, the phase variation
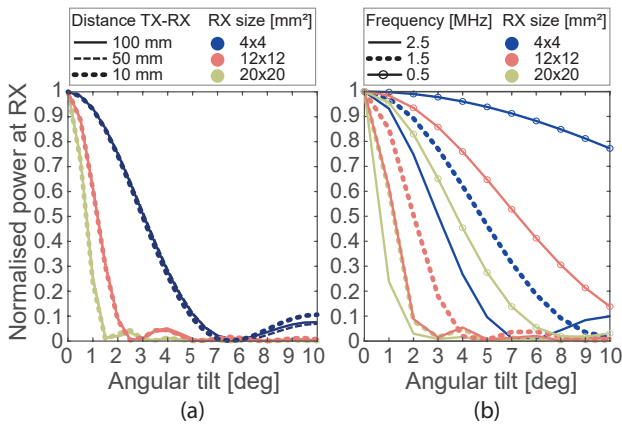

Fig. 3. Simulated effect of angular tilt of the RX on the harvestable power at the RX (a) depending on the receiver size and the distance; (b) depending on the frequency and receiver size.

across each array element becomes smaller. Figure 5 shows the improvement in usable power in relationship with the number of partitions for a 20×20 mm^2 RX placed at 50 mm distance from the TX. The improvement in usable power is defined in terms of relative efficiency, calculated as the ratio between the usable power to the power in case of no phase difference across the RX. The larger the angular misalignment, the higher the number of partitions necessary to recover a defined amount of power. In addition, the dashed line in Fig. 5 represents the effect of a virtual partitioning of the pressure field generated by the previously introduced PZT transducer. Virtual partitioning indicates the subdivision of the area scanned by the needle hydrophone in the same way as the simulations, and the gathering of the pressure values for the data points in each partition to calculate the usable power. Fig. 5 shows measurements and simulations in good agreement.

Partitioning the RX transducer comes however at the cost of increased complexity in packaging and matching circuitry. In fact, for this solution to work, each partition requires a rectifier such that the power harvested by each partition, and more specifically, the current generated by each partition, can be added together in the DC domain. In addition, to maximise the power transfer efficiency, a matching circuit is required, which usually comprises an inductor. While the rectifier can be embedded in the power management chip, the matching components are discrete and need to be connected to each partition, increasing the volume and complexity of the packaging. Inductors are bulky and may contain toxic materials, requiring a hermetic enclosure, such as Titanium (Ti). However, Ti would block the transfer of ultrasonic waves, requiring more advanced packaging methods such as conformal encapsulation [13], [14]. Hence, the number of partitions should be determined as a trade-off between the minimum

acceptable power loss due to misalignment and the added packaging complexity resulting from the need to electrically interconnect multiple transducers rather than a single element.

IV. Conclusion

In this work, we presented the effect of lateral and angular misalignment, demonstrating that the latter can significantly degrade the usable power, even for small tilts. We proposed a potential solution to mitigate this problem, which consists of partitioning the receiving transducer, showing that the larger the tilt angle, the higher the number of partitions necessary to recover a defined amount of power. However, the number of partitions should be chosen as a trade-off between the minimum acceptable power loss due to misalignment and the increased packaging and circuit complexity.

Acknowledgment

References

[1] V. Giagka and W. A. Serdijn, "Realizing flexible bioelectronic medicines for accessing the peripheral nerves–technology considerations," *Bioelectronic medicine*, vol. 4, no. 1, pp. 1–10, 2018.
[2] C. Shi, V. Andino-Pavlovsky, S. A. Lee, T. Costa, J. Elloian, E. E. Konofagou, and K. L. Shepard, "Application of a sub–0.1-mm^3 implantable mote for in vivo real-time wireless temperature sensing," *Sci Adv*, vol. 7, no. 19, 2021.
[3] A. Rashidi, N. Yazdani, and A. M. Sodagar, "Fully implantable, multi-channel microstimulator with tracking supply ribbon, multi-output charge pump and energy recovery," *IET Circuits, Devices & Systems*, vol. 15, no. 2, pp. 104–120, 2021.
[4] A. Rashidi, M. Zamani, T. Mondal, S. Hosseini, K. Laursen, B. Corbett, and F. Moradi, "Ultrasonically Powered and Controlled Microsystem for Dual-Wavelength Optogenetics With a Multiload Regulation Scheme," *IEEE Solid-State Circuits Letters*, vol. 6, pp. 33–36, 2023.
[5] J. Charthad, T. C. Chang, Z. Liu, A. Sawaby, M. J. Weber, S. Baker, F. Gore, S. A. Felt, and A. Arbabian, "A mm-Sized Wireless Implantable Device for Electrical Stimulation of Peripheral Nerves," *IEEE Transactions on Biomedical Circuits and Systems*, vol. 12, no. 2, pp. 257–270, 2018.
[6] S. Hosseini, K. Laursen, A. Rashidi, T. Mondal, B. Corbett, and F. Moradi, "S-MRUT: Sectored-Multiring Ultrasonic Transducer for Selective Powering of Brain Implants," *IEEE Transactions on Ultrasonics, Ferroelectrics, and Frequency Control*, vol. 68, no. 1, pp. 191–200, 2021.
[7] H. Rivandi and T. L. Costa, "A 2D Ultrasound Phased-Array Transmitter ASIC for High-Frequency US Stimulation and Powering," *IEEE Transactions on Biomedical Circuits and Systems*, pp. 1–12, 2023.
[8] L. Tacchetti, W. A. Serdijn, and V. Giagka, "An Ultrasonically Powered and Controlled Ultra-High-Frequency Biphasic Electrical Neurostimulator," in *2018 IEEE Biomedical Circuits and Systems Conference (BioCAS)*. IEEE, Oct. 2018.
[9] O. Wong, D. Tabruyn, V. Rochus, and N. Van Helleputte, "An Implantable Power Extraction Circuit with Integrated PMUTs for Wireless Power Delivery," in *ESSCIRC 2022- IEEE 48th European Solid State Circuits Conference (ESSCIRC)*, 2022, pp. 217–220.
[10] T. Zhang, H. Liang, Z. Wang, C. Qiu, Y. B. Peng, X. Zhu, J. Li, X. Ge, J. Xu, X. Huang, J. Tong, J. Ou-Yang, X. Yang, F. Li, and B. Zhu, "Piezoelectric ultrasound energy–harvesting device for deep brain stimulation and analgesia applications," *Science Advances*, vol. 8, no. 15, Apr. 2022.
[11] "FOCUS." [Online]. Available: https://www.egr.msu.edu/~fultras-web/
[12] B. Khuri-Yakub and O. Oralkan, "Energy harvesting," Patent US9 774 277B2, 26 Sept 2017.
[13] A. Pak, K. Nanbakhsh, O. Hölck, R. Ritasalo, M. Sousa, M. van Gompel, B. Pahl, J. Wilson, C. Kallmayer, and V. Giagka, "Thin Film Encapsulation for LCP-Based Flexible Bioelectronic Implants: Comparison of Different Coating Materials Using Test Methodologies for Life-Time Estimation," *Micromachines*, vol. 13, no. 4, p. 544, 2022.
[14] C. Lamont, T. Grego, K. Nanbakhsh, A. Shah Idil, V. Giagka, A. Vanhoestenberghe, S. Cogan, and N. Donaldson, "Silicone encapsulation of thin-film SiOx, SiOxNy and SiC for modern electronic medical implants: a comparative long-term ageing study," *Journal of Neural Engineering*, vol. 18, no. 5, p. 055003, 2021.
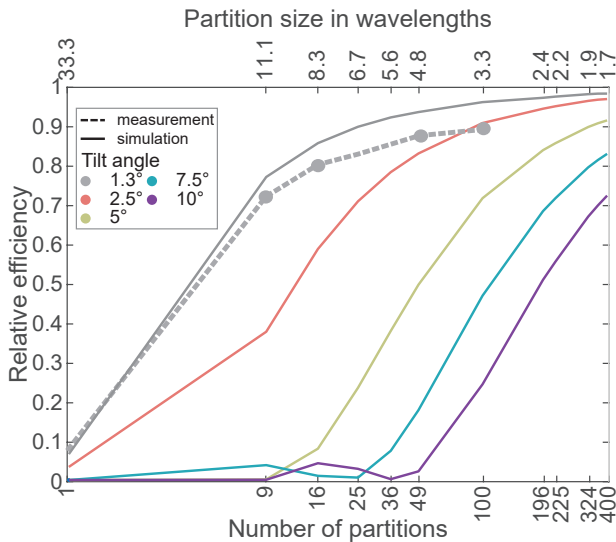

Fig. 5. Effect of partitioning on the usable power for a 20×20 mm^2 RX placed at 50 mm, for different angular misalignment. The solid line represents the results of the simulations. The dashed line represents the results from experimental data. The x-axis scale is logarithmic